Crystal structure and mechanism of a calcium-gated potassium channel

Youxing Jiang, Alice Lee, Jiayun Chen, Martine Cadene, Brian T. Chait & Roderick MacKinnon

Howard Hughes Medical Institute, Laboratory of Molecular Neurobiology and Biophysics and Laboratory of Mass Spectrometry and Gaseous Ion Chemistry, Rockefeller University, 1230 York Avenue, New York, New York 10021, USA

Ion channels exhibit two essential biophysical properties; that is, selective ion conduction, and the ability to gate-open in response to an appropriate stimulus. Two general categories of ion channel gating are defined by the initiating stimulus: ligand binding (neurotransmitter- or second-messenger-gated channels) or membrane voltage (voltage-gated channels). Here we present the structural basis of ligand gating in a K^+ channel that opens in response to intracellular Ca^{2+}. We have cloned, expressed, analysed electrical properties, and determined the crystal structure of a K^+ channel (MthK) from *Methanobacterium thermoautotrophicum* in the Ca^{2+}-bound, opened state. Eight RCK domains (regulators of K^+ conductance) form a gating ring at the intracellular membrane surface. The gating ring uses the free energy of Ca^{2+} binding in a simple manner to perform mechanical work to open the pore.

Ion channels are central to a wide range of biological processes including cell volume regulation, movement and electrical signal generation[1]. Ion channel proteins span the membrane of a cell, forming a conduction pathway, or pore, through which ions diffuse down their electrochemical gradient across the membrane. To understand how an ion channel operates as a molecular machine we addressed two mechanistic issues. First, how do ions flow selectively through the pore, and second, how does the pore gate, or open, in response to the appropriate stimulus? For K^+ ion channels, significant progress has been made towards understanding the mechanism of selective ion conduction[2–4]. Here we address the mechanism of opening in a ligand-gated K^+ channel.

K^+ channels belong to a family of ion channels called tetrameric cation channels. The family includes K^+, Na^+, Ca^{2+}, cyclic nucleotide-gated, and several other ion channels. They contain four membrane-spanning subunits or domains surrounding a central pore that is selective for cations of one kind or another. On the basis of the KcsA K^+ channel structure[2,4], it seems that cation selectivity is an intrinsic property of the pore architecture, which provides a special arrangement of cation-attractive 'pore' α-helices probably shared by all tetrameric cation channel family members.

Gating in the tetrameric cation channels is conferred through the attachment of gating domains to the pore. In channels whose gate opens in response to the membrane voltage (voltage-dependent channels), an integral membrane 'voltage sensor' domain is present on each subunit[5,6]. In ligand-gated channels, ligand-binding domains are attached to the pore in the aqueous solution near the membrane surface[7–11] (Fig. 1). The basic function of these gating domains is to perform mechanical work on the ion conduction pore to change its conformation between closed and opened states. Thus, a voltage sensor converts energy stored in the membrane electric field into mechanical work, whereas ligand-binding domains convert the free energy of ligand binding into mechanical work. Thus, ion channel gating comes down to electromechanical or chemomechanical coupling between a gating unit and the pore unit.

Regulators of K^+ conductance (RCK) domains are found in many ligand-gated K^+ channels, most often attached to the intracellular carboxy terminus (Fig. 2a)[11]. These domains are prevalent among prokaryotic K^+ channels, and are also found in eukaryotic, high-conductance Ca^{2+}-activated K^+ channels (BK channels). Several RCK domain amino-acid sequences are shown in Fig. 2a. The X-ray structure of one RCK domain, that from an *Escherichia coli* K^+ channel, reveals an α-β-protein with a fold similar to dehydrogenase enzymes[11]. The domain forms a homodimer, producing a cleft between two lobes. The dimer is similar in its structure to certain bi-lobed, amino acid and nutrient molecule-binding proteins found in the periplasm of bacteria[12–14]. We postulated that the *E. coli* K^+ channel binds a ligand molecule in the cleft to affect channel gating. On the basis of amino-acid sequence analysis it is apparent that certain RCK domains bind nicotinamide adenine dinucleotide (NAD)[15,16], but for many RCK domains the ligand is unknown.

Analysis of DNA sequences shows that RCK domains occur in at least five different contexts (Fig. 2b): (1) as a single domain on the C terminus of a K^+ channel (for example, many prokaryotic K^+ channels); (2) as two tandem RCK domains on the C terminus (for example, eukaryotic BK channels); (3) as two domains, one on the N and another on the C terminus; (4) as a soluble protein (not part of a K^+ channel gene) consisting of two tandem RCK domains; and (5) as a soluble protein consisting of a single RCK domain. Of note, in three out of five contexts (Fig. 2b, (2)–(4)), RCK domains occur in pairs.

The MthK channel

We cloned and expressed a K^+ channel gene from the archeon *Methanobacterium thermoautotrophicum*. The gene codes for a K^+ channel that we have named MthK; it contains two membrane-spanning segments per subunit, which forms one subunit of the transmembrane pore, and a single C-terminal RCK domain (Fig. 3a). Expression in *E. coli*, extraction with decylmaltoside

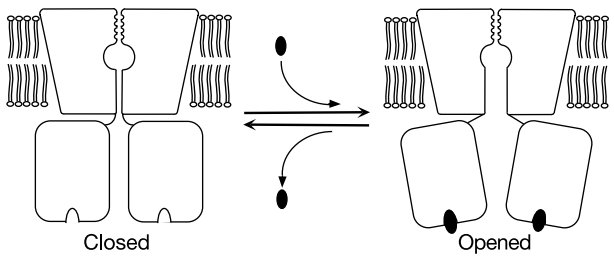

Figure 1 Ligand-activated ion channel gating. A ligand (black oval) binds to receptor domains, inducing a conformational change that leads to opening of the ion conduction pore. The ligand receptor is usually located at the membrane surface on the extracellular side (top) in neurotransmitter-gated ion channels and on the intracellular side (bottom) in second-messenger-gated ion channels, as shown here.

(DM), and purification yields a protein–detergent complex that elutes in a peak at approximately 11 ml on a superdex-200 (10/30) gel filtration column (Fig. 3b). Protein from this peak runs in two bands near a relative molecular mass of 26,000 and 200,000 (M_r 26K and 200K, respectively) on SDS–polyacrylamide gel electrophoresis (PAGE) (Fig. 3b). Mass spectrometry shows that the approximately 200K band contains the full-length gene product, presumably migrating as a tetramer on SDS–PAGE, and that the roughly 26K band contains only the C-terminal RCK domain, beginning at amino-acid position Met 107. In separate experiments we observed a similar result on overexpression of the *E. coli* K^+ channel in *E. coli*: two proteins were produced, one full length and another corresponding to a C-terminal RCK domain, beginning at an internal methionine residue. We reasoned that a single gene gives rise to two gene products, and that both products are required in the assembly of a functional K^+ channel (Fig. 3d). Mutation of the hypothesized internal start site, Met 107, to Ile (M107I) eliminated the 26K gene product (Fig. 3c) and resulted in reduced levels of MthK channel expression. Curiously, on the superdex-200 column the mutant channel elutes at approximately 10 ml, indicating that it is larger in size than the wild-type channel (Fig. 3c). The structural analysis below offers an explanation for this unexpected result; that two mutant channels bind to each other once they have been extracted from the membrane (Fig. 3e). Such binding would provide compensation for the missing soluble domains and explain the large protein–detergent complex on gel filtration.

Electrophysiological analysis

MthK channels produced with Met 107 intact were reconstituted into planar lipid bilayers of 1-palmitoyl-2-oleoyl phosphatidylglycerol (POPG) and 1-palmitoyl-2-oleoyl phosphatidylethanolamine (POPE) (Fig. 4). The channel is selective for K^+ over Na^+ (data not shown), and in solutions containing 150 mM KCl and 10 mM HEPES, pH 7.0 on both sides of the membrane it exhibits inward rectification: the current–voltage curve is nonlinear, with a greater slope at negative voltages (Fig. 4a). Single channels show a conductance of approximately 200 pS at −100 mV. The K^+ channel blocker charybdotoxin (CTX), a protein from scorpion venom[17], inhibits the MthK channel, underscoring the structural similarity between this prokaryotic K^+ channel and its eukaryotic family members (Fig. 4b). CTX binds to the extracellular pore entryway of K^+ channels[18], which allows easy assessment of a channel's orientation within the membrane, that is, it distinguishes the extracellular (toxin sensitive) and intracellular (toxin insensitive) sides.

Figure 4b shows an important property of the MthK channel. When Ca^{2+} is applied to the intracellular solution, the probability of channel opening increases (Fig. 4b). The '0 mM' Ca^{2+} recording contains trace amounts of Ca^{2+} necessary to open channels; in the presence of EDTA, a Ca^{2+} chelator, MthK channels essentially never open. Thus, Ca^{2+} regulates or gates the channel from the intracellular solution: the effect of Ca^{2+} continues into the millimolar concentration range. The reduced single-channel amplitude at higher Ca^{2+} concentrations is due to rapid pore block by Ca^{2+} ions, a well known phenomenon[19–21]. The principal result, however, is that Ca^{2+} gates the channel open. We do not know whether Ca^{2+} is a physiological ligand for gating the MthK channel, but for the purposes of the present study, Ca^{2+} is a ligand that opens the channel in a concentration-dependent manner.

X-ray structure analysis

We solved the three-dimensional structure of the MthK channel by X-ray crystallography at a resolution of 3.3 Å (Methods; see also

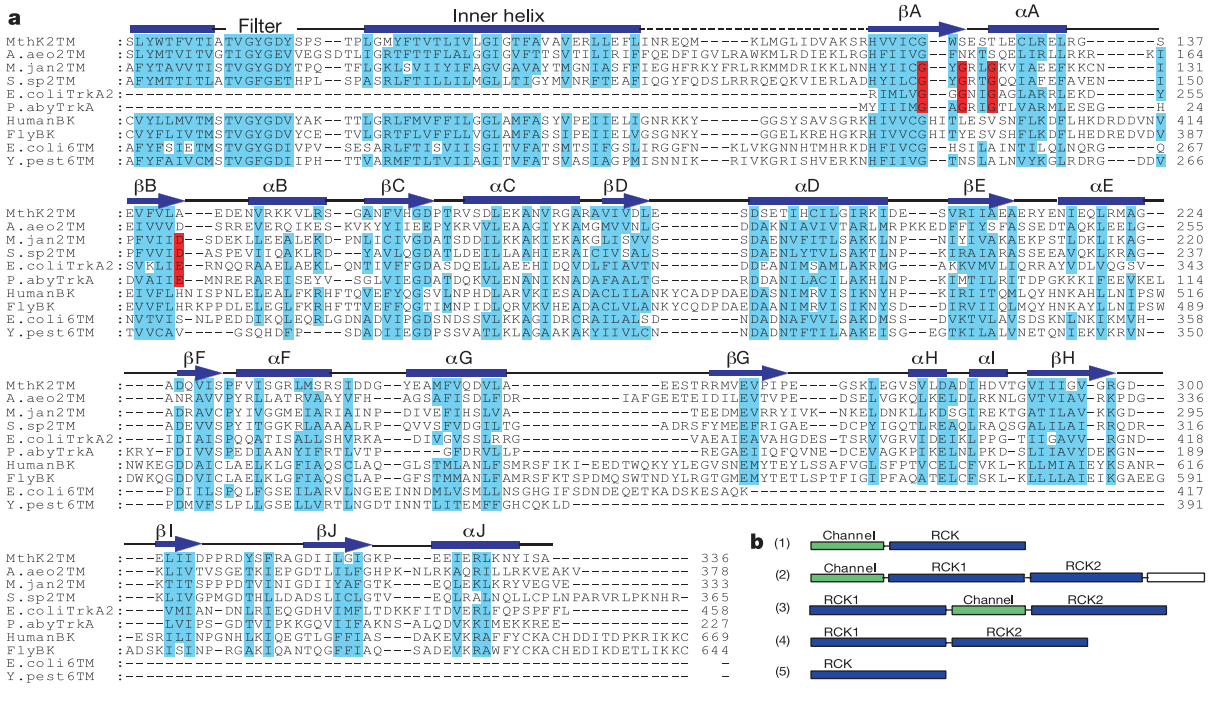

Figure 2 Sequence analysis of proteins containing RCK domains. **a**, Partial sequence alignment of K^+ channels and prokaryotic K^+ transporters (TrkA). The alignment begins at the K^+ channel signature sequence (Filter) and ends at the MthK channel (MthK2TM) C terminus. Secondary structure assignment is based on the MthK crystal structure: blue bars and arrows show α-helices and β-strands, respectively; dashed line shows the structurally undefined linker connecting the pore to the RCK domain. Cyan indicates semi-conserved sequence; red shows an NAD-binding motif present in some RCK domains. K^+ channels: MthK2TM, *M. thermautotrophicum* (GI:2622639); A.aeo2TM, *Aquifex aeolicus* (GI:2983007); M.jan2TM, *Methanococcus jannaschii* (GI:1498918); S.sp2TM, *S. sp* (GI:7447543); E.coli6TM, *E. coli* (GI 400124); Y.pest6TM, *Yersinia pestis* (sanger_632); TrkA proteins: E.coliTrkA2, *E. coli*, domain 2 (GI:136235); P.abyTrkA, *Pyrococcus abyssi* (GI:7450648); BK K^+ channels: HumanBK, *Homo sapiens* (GI:2570854); FlyBK, *Drosophila melanogaster* (GI:7301192). **b**, RCK domains: (1) single C-terminal domain of K^+ channels; (2) tandem C-terminal domains (BK channels); (3) N- and C-terminal domains (*Synechocystis* sp. channel); and (4) and (5) soluble containing tandem (*E. coli* TrkA) or single (*P. abyssi* TrkA) domains of prokaryotic K^+ transporters.

Supplementary Information Table 1). Crystals were obtained using the mutant M107I in which the proposed second start site was removed (Fig. 3a, c). Within a $P6_122$ crystal lattice, two channels are arranged in a 'back-to-back' fashion (Fig. 3e). From our biochemical studies (Fig. 3) and subsequent structural analysis we conclude that the back-to-back channels in the crystal share RCK domains, and that a functional K^+ channel corresponds to the diagram in Fig. 3d. Thus, in the membrane an MthK channel apparently has eight RCK domains at its intracellular surface, four co-assembling from solution. We refer to the membrane-spanning portion of the MthK channel as the pore, and the structure formed by the eight RCK domains as the gating ring.

The electron density map in the region of the gating ring is of high quality, enabling us to build nearly all amino-acid side chains. The pore is not as well ordered in the crystal, but four-fold noncrystallographic symmetry (NCS) averaging provided good definition of the main chain helical structure. The pore was built as a polyalanine model, but density for the largest side chains and sequence analysis permitted the unambiguous assignment of the helical register within the pore. The final MthK channel model (R_{cryst}, 29.9%; R_{free}, 31.5%) is built from amino acids 19–336, with the exception of 17 unresolved residues (99–115) at the junction between the pore and the gating ring (Fig. 5a).

A surface-rendered structure of the MthK channel with one subunit removed is shown with the membrane-spanning pore above and the intracellular gating ring below (Fig. 5b). The entire channel, pore and gating ring, shares four-fold symmetry by rotation of the unit shown in Fig. 5a about the pore axis. The gating ring is large (approximately 1,800 amino acids) compared with the pore (about 400 amino acids), and the hole down the centre of the gating ring is approximately 20 Å in diameter, providing a wide path for the movement of K^+ ions between the cytoplasm and the pore.

The crystals were grown in the presence of 200 mM Ca^{2+}, a ligand that opens the channel in electrophysiological experiments (Fig. 4b). Well defined peaks in the electron density map are most consistent with Ca^{2+} ions on the basis of local chemistry; these ions are shown as yellow spheres lining the wall inside the gating ring (Fig. 5b). Two Ca^{2+} ions are located at the base of a cleft between two RCK domains (Fig. 5a), coordinated by the carboxylate groups of glutamate residues 210 and 212, and by aspartate residue 184 (Fig. 5c). To test whether these Ca^{2+} ions in the structure are directly correlated with channel gating, we mutated Asp 184 to Asn in the Ca^{2+} binding site, and reconstituted the mutant channel (Met 107 intact) into lipid bilayers. Channel gating was affected signifi-

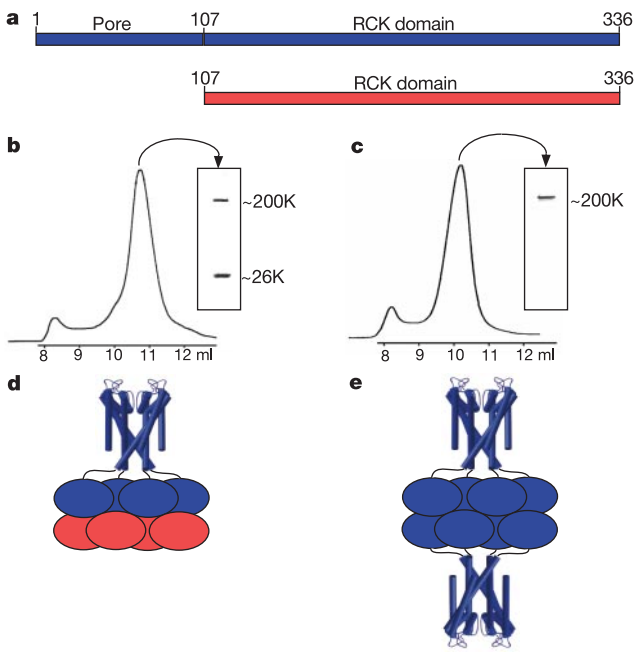

Figure 3 Biochemical analysis of MthK. **a**, Expression of wild-type MthK yields two proteins: full-length channel (blue bar) and the RCK domain from Met 107 (red bar). **b**, Gel-filtration profile and SDS–PAGE of wild-type MthK purified in DM. Major peak elutes at 10.7 ml (superdex-200, 10/30); protein from this peak migrates as two bands on SDS–PAGE (inset) at 26K (RCK domain) and about 200K (MthK tetramer). **c**, Gel-filtration profile and SDS–PAGE of MthK mutant M107I purified in DM. Major peak elutes at 10.2 ml; protein from this peak migrates as a single band on SDS–PAGE (inset) at about 200K (MthK tetramer). **d**, **e**, Hypothesis explaining the biochemical results for wild-type (**d**) and M107I mutant (**e**) channel expression. Pore is shown as cylinders and RCK domains as ovals with colours as in **a**.

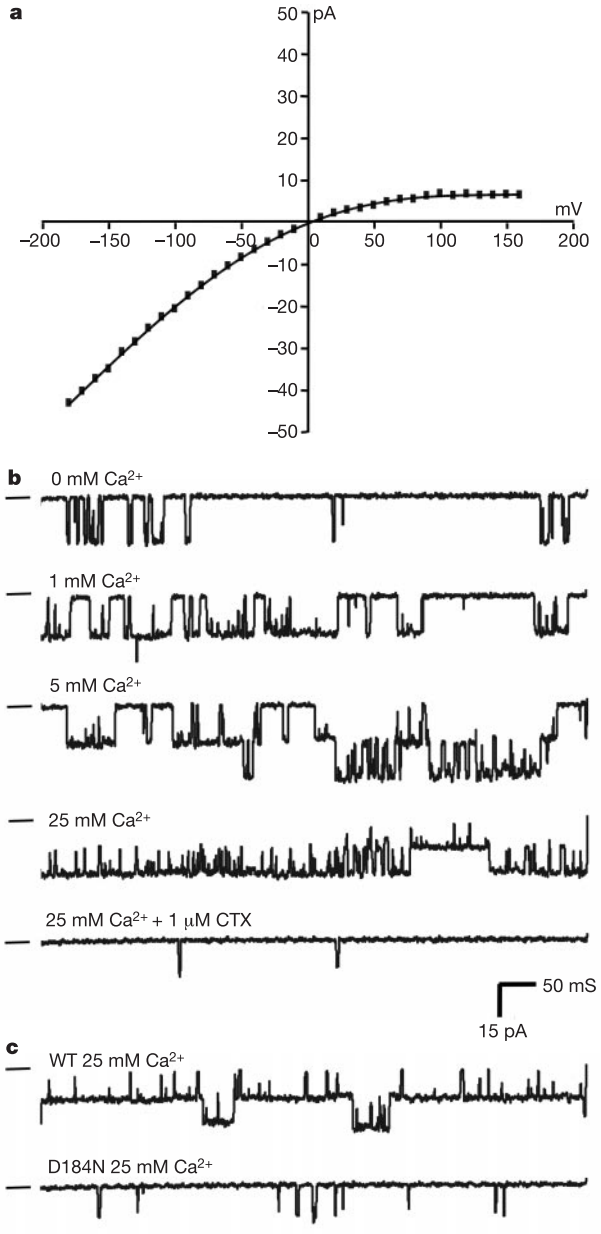

Figure 4 Electrophysiological analysis of MthK in lipid bilayers. **a**, Current–voltage curve of MthK measured in solutions of 150 mM KCl, 10 mM HEPES, pH 7.0, on both sides of the membrane. **b**, Single channel traces of MthK in response to various internal Ca^{2+} concentrations or external CTX. Membrane voltage was −100 mV so that channel openings cause a downward current; lines to the left mark the zero current level. **c**, Single channel traces of wild-type (WT) MthK and D184N mutant in the presence of 25 mM internal Ca^{2+}, 150 mM KCl, 10 mM HEPES, pH 7.0.

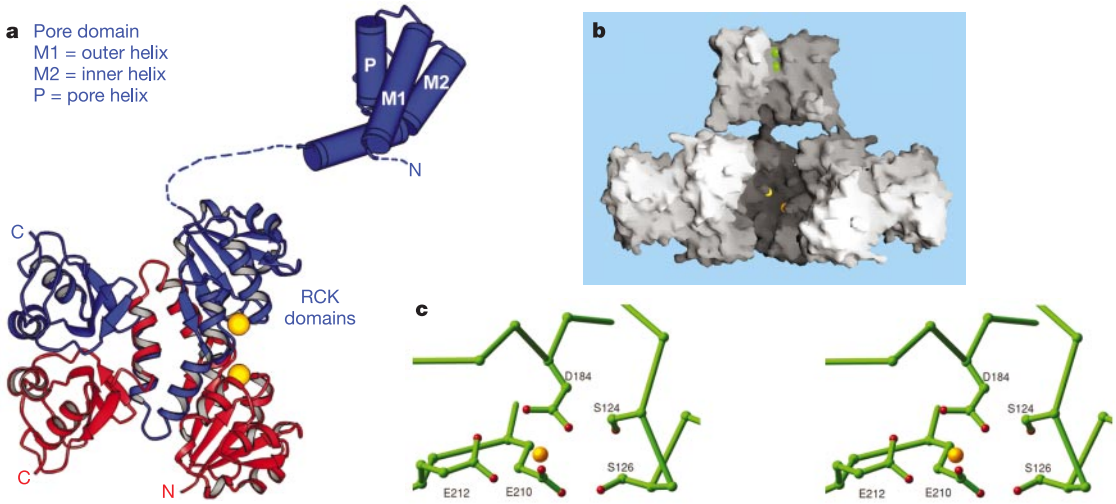

Figure 5 Structure of the MthK K^+ channel. **a**, A single four-fold repeated unit of the MthK channel contains a pore domain (blue cylinders) and two RCK domains (blue and red ribbons). Disordered segments (dashed) and Ca^{2+} ions (yellow spheres) are shown. **b**, Molecular surface of the MthK tetramer viewed from the side (extracellular surface on top) with one unit removed. Green and yellow spheres show K^+ and Ca^{2+} ions, respectively. **c**, Stereo diagram of the Ca^{2+}-binding site with protein atoms in green and red and Ca^{2+} in yellow. All ribbon diagrams were prepared using RIBBONS[39] and all surface models using GRASP[40].

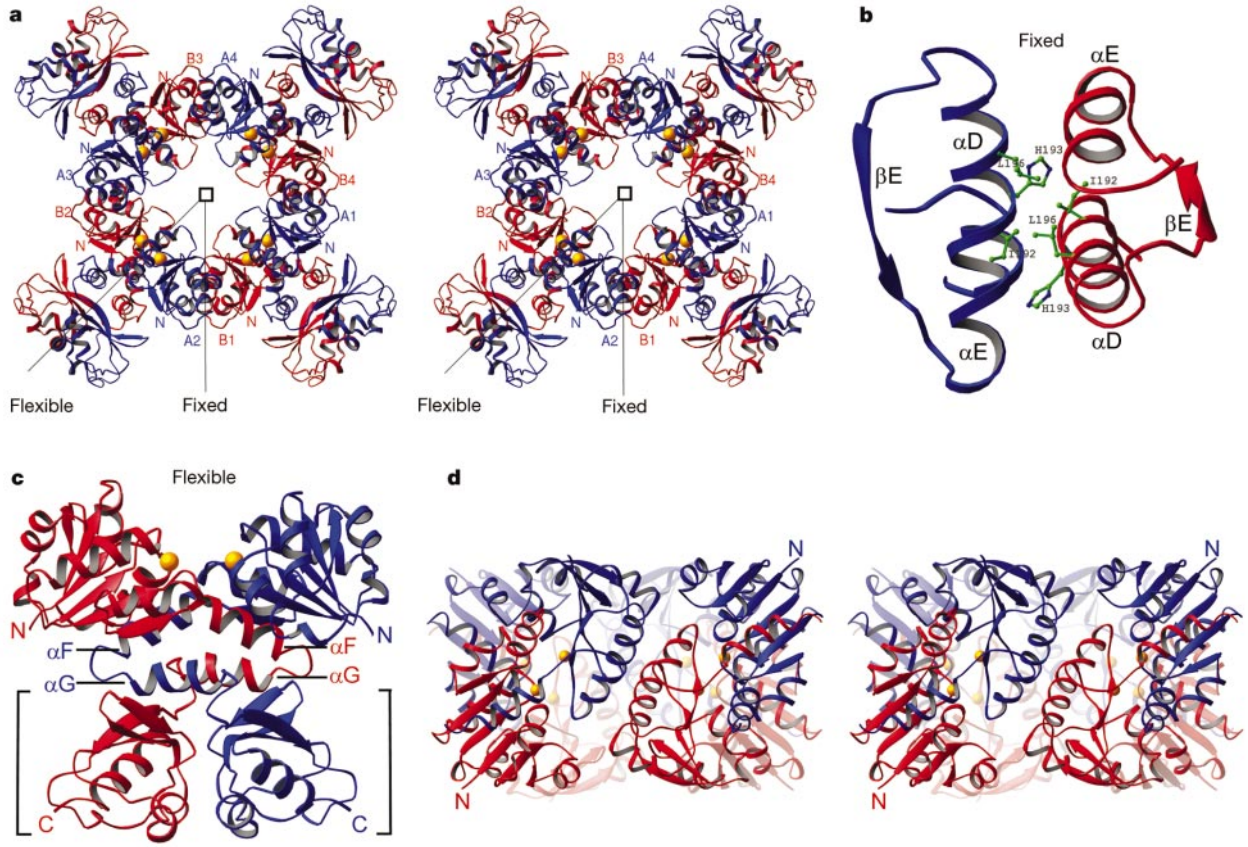

Figure 6 Structure of the gating ring. **a**, Stereo diagram of the gating ring viewed down the four-fold axis (square). Eight RCK domains are divided into two groups, A1–A4 (blue) and B1–B4 (red), with N termini labelled (N). Viewed from the membrane, blue domains would be attached to the pore via a continuous polypeptide chain and red domains assembled from solution. Fixed and flexible dimer interfaces hold the ring together. **b**, Helices αD and αE form the fixed interface. Several amino acids conserved as hydrophobic or aromatic (Ile 192, His 193 and Leu 196) are shown. **c**, C-terminal subdomains (brackets) and helices αF and αG form the flexible interface. A cleft between two RCK domains creates a ligand-binding site with Ca^{2+} bound at the base (yellow spheres). **d**, Stereo diagram of the gating ring viewed from the side after removing the subdomains.

cantly by this mutation (Fig. 4c). In particular, at a high Ca^{2+} concentration the mean open time was short and the mean closed time long compared with the wild-type channel, resulting in an apparent decrease in the ability of Ca^{2+} to open the channel. We conclude that by binding to its sites in the cleft between RCK domains in the gating ring, Ca^{2+} causes the MthK channel to open. Our crystal structure shows the gating ring in its Ca^{2+}-bound conformation that would favour pore opening. Not surprisingly, the pore of the MthK channel in the crystal is wide open: the arrangement of inner helices is very different from that observed in the KcsA K^+ channel[22].

The gating ring

The gating ring has an arrangement of eight identical RCK domains (Fig. 6a). If one imagines that the blue domains—nearest the viewer in Fig. 6a—are attached to the membrane pore through the polypeptide chain, then the red domains come from solution. The complementary interlocking of blue and red domains to form the closed ring shows why a functional MthK channel apparently requires eight RCK domains: blue domains never directly contact blue domains; similarly, red never contact red.

Two unique protein interfaces between blue and red domains hold the ring together. We have called one of these the fixed interface. The fixed interface is formed by helices αD and αE (Fig. 6a, b). Based on the conservation of specific hydrophobic amino acids on helix αD, we think that the fixed interface occurs in nearly all RCK domains. We call the other protein interface flexible (Fig. 6a, c). The flexible interface is formed in part by the subdomains that protrude out from the gating ring, and in part by helices αG and αF. The peripheral subdomain is variable among RCK domains, and appears to be a unit that adds stability to the flexible interface (Fig. 6c, brackets). The crucial and conserved (among RCK domains) aspect of the flexible interface is not the peripheral subdomain, but the region where the ligand-binding cleft is formed between main lobes of two adjacent RCK domains (Fig. 6c, top). This interface forms the Ca^{2+}-binding cleft in the MthK channel-gating ring.

It is instructive to view the gating ring from the side after removing the peripheral subdomains (Fig. 6d). From this perspective, the alternating arrangement of RCK domains is visible. Going around the ring, left to right on the front face, a blue domain is attached to a red domain through a fixed interface, the red domain is then attached to a blue domain by a flexible interface. This pattern of fixed and flexible interfaces repeats itself around the ring.

A mechanism for Ca^{2+}-activation

How might the gating ring convert the free energy of Ca^{2+} binding into mechanical work on the pore? To address this question, we compared RCK domain structures (without their peripheral subdomains) from the MthK and *E. coli* K^+ channels (Fig. 7). The RCK domain from the MthK channel is from the complete channel structure, solved with Ca^{2+} ions in the ligand-binding site, whereas the *E. coli* channel RCK domain was solved separately from the channel and is without a ligand[11]. Despite these differences, the same two domain–domain interfaces, fixed and flexible, occur in both crystals, but with notable variation. Across the fixed interface, two RCK domains of the MthK channel (Fig. 7a, black) have the same relative relationship to each other as two *E. coli* channel RCK domains (Fig. 7a, red). That is, two RCK domains across this interface are fixed with respect to each other. Across the flexible interface, however, there are large structural differences: the ligand-binding cleft is relatively closed between two MthK channel RCK domains (Fig. 7b, black), and open between two *E. coli* channel RCK domains (Fig. 7b, red). Several reasons can account for the relative movements at the flexible interface: forces imposed by unique crystal lattices, the constraint of being attached to a channel and held in a ring, and the presence of a ligand. The important point is, comparison of the two different crystals indicates that one RCK domain interface is fixed and the other is clearly flexible. Moreover, the flexible hinge, which allows movement, occurs at the base of the cleft near to where Ca^{2+} binds in the MthK channel. One can imagine Ca^{2+} influencing the structure by binding in the cleft. In bacterial periplasmic-binding proteins[12–14] and glutamate receptor ligand-binding domains[23,24], this is exactly what happens; a ligand binds in the cleft between two domains and causes the domains to move relative to each other.

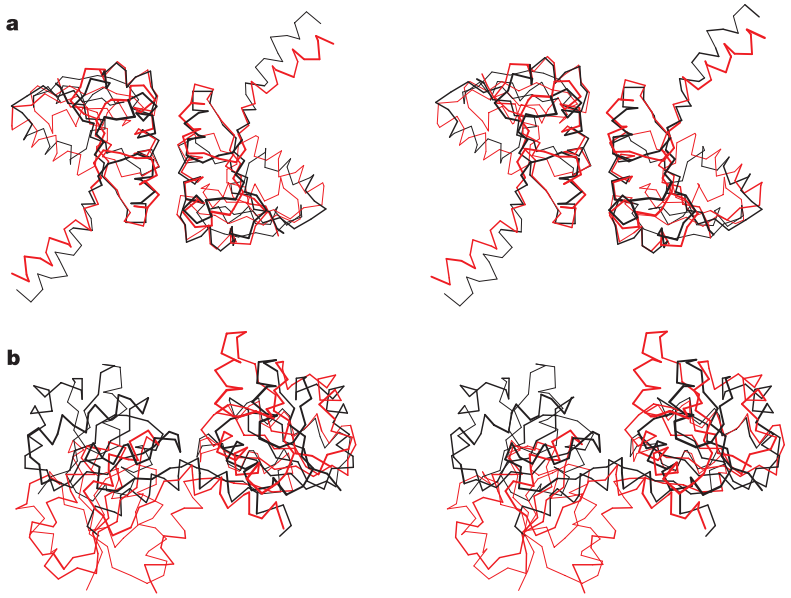

Figure 7 Comparison of different RCK domains reveals possible gating motions. **a**, **b**, RCK domains from the MthK channel (PDB code 1LNQ), residues 116–245 (black Cα trace), and the *E. coli* K^+ channel (PDB code 1ID1), residues 244–379 (red Cα trace), are superimposed, showing the fixed (**a**) and flexible (**b**) dimer interfaces in stereo. Across the fixed interface both dimer halves are simultaneously superimposable. Across the flexible interface only one half can be superimposed at once due to relative domain movements. The figures were prepared using Bobscript[41].

The static compared with dynamic property of the two interfaces offers a plausible explanation for how the gating ring could open and close the channel. In Fig. 8a the crystal structure of the complete MthK channel is shown from the side. The peripheral subdomains have been removed from the gating ring to simplify the picture, and dashed lines show the expected path of the unresolved connection between the pore and gating ring. RCK domains on either side of a fixed interface are the same colour to reinforce the idea that such pairs are stuck rigidly together, and are expected to move as a single rigid unit. Viewed in this way, the gating ring can be described as an assembly of four rigid units (RCK domain pairs attached by the fixed interface), tilted and packed in a left-handed 'bundle'. In principle, the shape of the gating ring is adjustable. To see how, imagine that each rigid unit is rotated about an axis through the fixed interface (coincident with the line labelled 'fixed' in Fig. 6a), and pushed towards the centre of the ring, as shown in Fig. 8b, c; then the entire gating ring will become taller and its diameter reduced (see movie in Supplementary Information). For such rigid unit movements to occur, the flexible interfaces that connect the rigid units around the ring would have to undergo a conformational change. We propose that this is the essence of the machine: movements of the rigid units will reshape the cleft and presumably influence the Ca^{2+} binding affinity, which is energetically equivalent to saying that Ca^{2+} binding will influence movements of the rigid units. We propose that the gating ring converts the free energy of ligand binding into mechanical work in just this way: Ca^{2+} binds and reshapes the cleft, causing the rigid units to tilt, which in turn expands the diameter of the gating ring and pulls open the pore's inner helices. The manual rigid conformational change shown in Fig. 8b was made without producing large steric clashes and reduces the diameter of the gating ring by about 13 Å. The change in ring diameter is of the correct magnitude to account for the structural differences observed between the inner helices of MthK (an opened channel) and KcsA (a closed channel), as described in ref. 22.

Ligand-induced activation of ion channels often occurs with a high degree of cooperativity[25]. A structural basis for understanding cooperativity is apparent in the proposed mechanism of the gating ring. When Ca^{2+} binds in one cleft to reshape its structure, the structure of adjacent clefts must also change through movements of the rigid units. Thus, Ca^{2+} binding at one site will have energetic consequences for Ca^{2+} binding to neighbouring sites, giving rise to cooperativity.

The gating ring in MthK channels is assembled from eight RCK domains, one from each of the four pore-forming subunits and four from the intracellular solution. One can imagine in some cases that the four RCK domains from solution might arise from a separate gene coding for an RCK domain. Indeed, there are many prokaryotic genes coding for single, soluble RCK domains. Perhaps some of

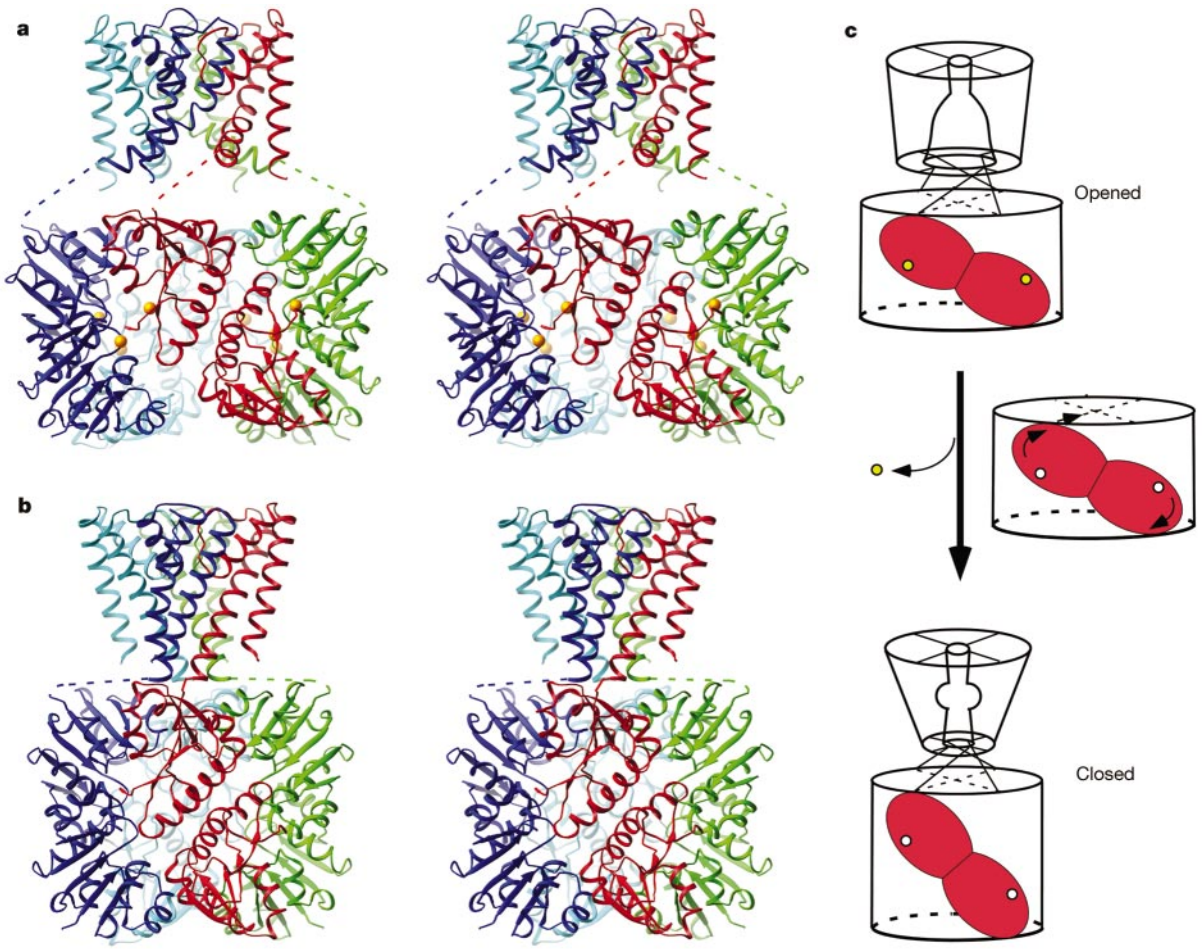

Figure 8 Proposed mechanism of gating. **a**, Crystal structure of the MthK channel (opened conformation) with subdomains removed from the gating ring. RCK domains forming a fixed interface with each other are the same colour. Disordered linkers are shown as dashed lines and Ca^{2+} ions as yellow spheres. **b**, Hypothetical model of the MthK channel in its closed conformation. RCK domain pairs of the same colour were moved as rigid bodies. The movements decrease the gating ring diameter by 13 Å, allowing the inner helices to achieve the conformation observed in the KcsA K^+ channel (a closed K^+ channel). **c**, Cartoon outlining the gating motions. A single rigid unit is shown (red). Arrows show proposed direction of rotation and translation. Release of Ca^{2+} ions (yellow circles) is associated with conformational changes in the gating ring that close the channel.

these domains assemble to form heteromultimer channels with unique ligand-gating properties. Yet another variation on the gating ring apparently occurs in eukaryotic BK channels. These Ca^{2+}-activated K^+ channels have a pair of tandem RCK domains on their C terminus. Therefore, eight RCK domains provided by the four channel subunits probably form a gating ring similar to that in the MthK channel. BK channels have an additional C-terminal domain, following the second RCK domain, which is also important for Ca^{2+}-activation[9].

Discussion

We have addressed the question of how the binding of a ligand is able to open the pore of an ion channel. We cloned, expressed, studied electrophysiological properties, and determined the crystal structure of a K^+ channel that contains RCK domains, and that is gated by intracellular Ca^{2+} ions. Calcium ions are present in the structure and the channel is in the open conformation. By interacting through two unique protein–protein interfaces, one fixed and the other flexible, eight RCK domains assemble to form a gating ring at the intracellular membrane surface. Through ligand-induced conformational changes at the flexible interface, we propose that the gating ring changes its shape in such a way that it can perform work on the pore, pulling open the inner helices to permit ion conduction. The gating ring is an example of how a seemingly complicated function—the opening of an ion channel through specific ligand binding—is carried out through a simple set of structural rules. □

Methods

Protein preparation and analysis

The gene coding for the MthK K^+ channel was cloned by polymerase chain reaction (PCR) amplification of genomic DNA from *M. thermoautotrophicum* (ATCC). The gene was inserted into the protein expression vector pQE70 (Qiagen) between *Sph*I and *Bgl*II restriction endonuclease sites with a thrombin cleavage site between a C-terminal hexahistidine sequence and the channel. In a mutated version of the gene, site-directed mutagenesis using QuickChange (Stratagene) was used to replace Met 107 with Ile (M107I mutant). For crystallization, the M107I mutant was expressed in *E. coli* SG13009 (pREP4) cell cultures on induction with 0.4 mM isopropyl-β-D-thiogalactopyranoside (IPTG). Expressed protein was extracted from cell lysate using 40 mM decylmaltoside (DM) and purified on a Talon Co^{2+} affinity column (Clontech). The protein was maintained in a solution of 5 mM DM, 20 mM Tris, pH 8.0 and 100 mM KCl. Nonspecifically bound protein was washed using 20 mM imidazole added to the above buffer, and the channel was then eluted with 300 mM imidazole. Immediately after elution, 1.0 unit of thrombin (Roche) per 3.0 mg channel was added to cleave the hexahistidine sequence overnight at room temperature. Protein was concentrated to about 15 mg ml^{-1}, run on a Superdex-200 (10/30) column (Pharmacia) in 5 mM N,N-dimethyldodecylamine-*N*-oxide (LDAO), 20 mM Tris, pH 8.0 and 100 mM KCl, and concentrated to 15.0 mg ml^{-1} (Centricon YM-50) for crystallization. For bilayer experiments, the same preparation was carried out using the wild-type channel and a mutant of the wild-type channel (D184N), except in the final gel filtration step where 5.0 mM DM detergent was used. Maldi time-of-flight mass spectrometry[26,27] (PerSeptive Biosystems Voyager-STR) was used to confirm that the wild-type MthK channel contains two polypeptides corresponding to full length and a partial length from position 107 to 336.

Crystallization

Crystals were grown by sitting-drop vapour diffusion at 20 °C by mixing equal volumes of protein and reservoir which contained 23–26% polyethylene glycol 350 monomethyl ether (PEGMME), 100 mM MES, pH 6.5 and 200 mM $CaCl_2$. Crystals were of space group $P6_122$, with cell dimensions $a = b = 137$ Å, $c = 373$ Å, $\alpha = \beta = 90°$ and $\gamma = 120°$, and four subunit copies in the asymmetric unit. Cryoprotection was achieved by raising the PEGMME concentration to about 40% by addition to the reservoir, after which crystals were frozen in liquid propane.

Structure determination

Data were collected at −180 °C under nitrogen stream. Numerous crystals were studied to obtain the best achievable diffraction data. The native data set used in the structure refinement was obtained at the National Synchrotron Light Source (NSLS) X-25 on a single crystal from protein in which residue 76 was mutated to cysteine; whether the mutation was responsible for modestly improved diffraction is unclear. The initial phases were estimated from CH_3HgCl derivative data collected at the Advanced Light Source (ALS) 5.0.2. All data sets were processed with DENZO and SCALEPACK[28]. Heavy atom positions for a first derivative were determined by Patterson search using SOLVE[29] and by direct methods using SnB[30], and for two additional derivatives using difference Fourier methods (CCP4 (ref. 31)). Heavy atom positions were refined and phases calculated using MLPHARE[31] and SHARP[32]; initial phases were improved by solvent flattening with SOLOMON[33]. Model building was aided by identifying the location of RCK domains in the electron density map with FFFEAR[34] using the *E. coli* RCK domain (Protein Data Bank code 1ID1, main chain from 241 to 365) as a search model[11]. Noncrystallographic symmetry (NCS) operators for the RCK domains were determined and subsequent four-fold averaging using RAVE[35] allowed phase extension from 4.2 Å to 3.3 Å. The NCS operators for the pore were slightly different than for the RCK domains so that the two regions of the electron density map were averaged separately. The model was built using O[36] and refinement carried out using CNS[37] by iterative cycles of simulated annealing with torsion-angle dynamics and model rebuilding. For convenience, the structure was refined against data reduced to space group $P6_1$, with two complete tetramers in the asymmetric unit. Strong NCS constraints were maintained throughout refinement. Electron density for the RCK domains was high quality, allowing the construction of a complete model from position 116 to 336, including Ca^{2+} ions. The pore was less well defined and built as a polyalanine model from position 19 to 98. The N-terminal 18 residues and residues from 99 to 115 were disordered. The final model contains 16,896 protein atoms, 8 Ca^{2+} ions, 4 K^+ ions, and is refined to R_{cryst} and R_{free} of 29.9% and 31.5%, respectively.

Single channel analysis

Wild-type MthK channels and the mutant D184N were reconstituted from DM into lipid vesicles as described[38], to give a final protein concentration of 100 μg ml^{-1}. Planar lipid bilayers of POPE (15 mg ml^{-1}) and POPG (5 mg ml^{-1}) in decane were painted over a 300-μm hole in a polystyrene partition separating internal and external solutions. To induce fusion of channel-containing vesicles, solution on the side to which vesicles were added (*cis*) contained 150 mM KCl, 10 mM HEPES, pH 7.0 and the opposite side (*trans*) contained 15 mM KCl, 10 mM HEPES, pH 7.0. After the appearance of channels in the membrane, KCl concentration on the *trans* side was increased to 150 mM. Charybdotoxin was used to define the extracellular side of the channel, and Ca^{2+} concentration was varied on the intracellular side. Membrane voltage was controlled and current recorded using an Axopatch 200B amplifier with a Digidata 1322A analogue-to-digital converter and Axoclamp software (Axon Instrument).

Received 22 March; accepted 22 April 2002.

1. Hille, B. *Ion Channels of Excitable Membranes* (Sinauer, Sunderland, Massachusetts, 2001).
2. Zhou, Y., Morais-Cabral, J. H., Kaufman, A. & MacKinnon, R. Chemistry of ion coordination and hydration revealed by a K^+ channel–Fab complex at 2.0 Å resolution. *Nature* **414,** 43–48 (2001).
3. Morais-Cabral, J. H., Zhou, Y. & MacKinnon, R. Energetic optimization of ion conduction rate by the K^+ selectivity filter. *Nature* **414,** 37–42 (2001).
4. Doyle, D. A. *et al.* The structure of the potassium channel: molecular basis of K^+ conduction and selectivity. *Science* **280,** 69–77 (1998).
5. Sigworth, F. J. Voltage gating of ion channels. *Q. Rev. Biophys.* **27,** 1–40 (1994).
6. Bezanilla, F. The voltage sensor in voltage-dependent ion channels. *Physiol. Rev.* **80,** 555–592 (2000).
7. Zagotta, W. N. & Siegelbaum, S. A. Structure and function of cyclic nucleotide-gated channels. *Annu. Rev. Neurosci.* **19,** 235–263 (1996).
8. Finn, J. T., Grunwald, M. E. & Yau, K. W. Cyclic nucleotide-gated ion channels: an extended family with diverse functions. *Annu. Rev. Physiol.* **58,** 395–426 (1996).
9. Schreiber, M. & Salkoff, L. A novel calcium-sensing domain in the BK channel. *Biophys. J.* **73,** 1355–1363 (1997).
10. Xia, X. M. *et al.* Mechanism of calcium gating in small-conductance calcium-activated potassium channels. *Nature* **395,** 503–507 (1998).
11. Jiang, Y., Pico, A., Cadene, M., Chait, B. T. & MacKinnon, R. Structure of the RCK domain from the *E. coli* K^+ channel and demonstration of its presence in the human BK channel. *Neuron* **29,** 593–601 (2001).
12. Sack, J. S., Saper, M. A. & Quiocho, F. A. Periplasmic binding protein structure and function. Refined X-ray structures of the leucine/isoleucine/valine-binding protein and its complex with leucine. *J. Mol. Biol.* **206,** 171–191 (1989).
13. Zou, J. Y., Flocco, M. M. & Mowbray, S. L. The 1.7 Å refined X-ray structure of the periplasmic glucose/galactose receptor from *Salmonella typhimurium*. *J. Mol. Biol.* **233,** 739–752 (1993).
14. Bjorkman, A. J. *et al.* Probing protein-protein interactions. The ribose-binding protein in bacterial transport and chemotaxis. *J. Biol. Chem.* **269,** 30206–30211 (1994).
15. Bellamacina, C. R. The nicotinamide dinucleotide binding motif: a comparison of nucleotide binding proteins. *FASEB J.* **10,** 1257–1269 (1996).
16. Schlosser, A., Hamann, A., Bossemeyer, D., Schneider, E. & Bakker, E. P. NAD+ binding to the *Escherichia coli* K(+)-uptake protein TrkA and sequence similarity between TrkA and domains of a family of dehydrogenases suggest a role for NAD+ in bacterial transport. *Mol. Microbiol.* **9,** 533–543 (1993).
17. Miller, C., Moczydlowski, E., Latorre, R. & Phillips, M. Charybdotoxin, a protein inhibitor of single Ca^{2+}-activated K^+ channels from mammalian skeletal muscle. *Nature* **313,** 316–318 (1985).
18. MacKinnon, R. & Miller, C. Mutant potassium channels with altered binding of charybdotoxin, a pore-blocking peptide inhibitor. *Science* **245,** 1382–1385 (1989).
19. Moczydlowski, E. & Latorre, R. Gating kinetics of Ca^{2+}-activated K^+ channels from rat muscle incorporated into planar lipid bilayers. Evidence for two voltage- dependent Ca^{2+} binding reactions. *J. Gen. Physiol.* **82,** 511–542 (1983).
20. Vergara, C. & Latorre, R. Kinetics of Ca^{2+}-activated K^+ channels from rabbit muscle incorporated into planar bilayers. Evidence for a Ca^{2+} and Ba^{2+} blockade. *J. Gen. Physiol.* **82,** 543–568 (1983).
21. Cox, D. H., Cui, J. & Aldrich, R. W. Separation of gating properties from permeation and block in mslo large conductance Ca-activated K^+ channels. *J. Gen. Physiol.* **109,** 633–646 (1997).
22. Jiang, Y. *et al.* The open pore conformation of potassium channels. *Nature* **417,** 523–526 (2002).
23. Mayer, M. L., Olson, R. & Gouaux, E. Mechanisms for ligand binding to GluR0 ion channels: crystal structures of the glutamate and serine complexes and a closed apo state. *J. Mol. Biol.* **311,** 815–836 (2001).
24. Armstrong, N., Sun, Y., Chen, G. Q. & Gouaux, E. Structure of a glutamate-receptor ligand-binding core in complex with kainate. *Nature* **395,** 913–917 (1998).
25. Golowasch, J., Kirkwood, A. & Miller, C. Allosteric effects of Mg^{2+} on the gating of Ca^{2+}-activated K^+ channels from mammalian skeletal muscle. *J. Exp. Biol.* **124,** 5–13 (1986).

26. Cadene, M. & Chait, B. T. A robust, detergent-friendly method for mass spectrometric analysis of integral membrane proteins. *Anal. Chem.* **72,** 5655–5658 (2000).
27. Cohen, S. L. & Chait, B. T. Mass spectrometry as a tool for protein crystallography. *Ann. Rev. Biophys. Biomol. Struct.* **30,** 67–85 (2001).
28. Otwinowski, Z. & Minor, W. Processing of X-ray diffraction data collected in oscillation mode. *Methods Enzymol.* **276,** 307–326 (1997).
29. Terwilliger, T. C. & Berendzen, J. Automated MAD and MIR structure solution. *Acta Crystallogr. D* **55 4,** 849–861 (1999).
30. Weeks, C. M. & Miller, R. The design and implementation of SnB version 2.0. *J. Appl. Cryst.* **32,** 120–124 (1999).
31. Collaborative Computational Project No. 4 The CCP4 suite: programs for X-ray crystallography. *Acta Crystallogr. D* **50,** 760–763 (1994).
32. de La Fortelle, E. & Bricogne, G. Maximum-likelihood heavy-atom parameter refinement for multiple isomorphous replacement and multiwavelength anomalous diffraction methods. *Methods Enzymol.* **276,** 472–494 (1997).
33. Abrahams, J. P. & Leslie, A. G. W. Methods used in the structure determination of bovine mitochondrial F1 ATPase. *Acta Crystallogr. D* **52,** 30–42 (1996).
34. Cowtan, K. Modified phased translation functions and their application to molecular-fragment location. *Acta Crystallogr. D* **54 5,** 750–756 (1998).
35. Kleywegt, G. J. & Jones, T. A. in *From the First Map to Final Model* Proceedings of the CCP4 study weekend (eds Bailey, S., Hubbard, R. & Waller, D.) 59–66 (Daresbury Laboratory, Daresbury, 1994).
36. Jones, T. A., Zou, J. Y., Cowan, S. W. & Kjeldgaard, M. Improved methods for building protein models in electron density maps and the location of errors in these models. *Acta Crystallogr. A* **47,** 110–119 (1991).
37. Brunger, A. T. *et al.* Crystallography & NMR system: a new software suite for macromolecular structure determination. *Acta Crystallogr. D* **54,** 905–921 (1998).
38. Heginbotham, L., LeMasurier, M., Kolmakova-Partensky, L. & Miller, C. Single streptomyces lividans K^+ channels. Functional asymmetries and sidedness of proton activation. *J. Gen. Physiol.* **114,** 551–560 (1999).
39. Carson, M. Ribbons. *Methods Enzymol.* **277,** 493–505 (1997).
40. Nicholls, A., Sharp, K. A. & Honig, B. Protein folding and association: insights from the interfacial and thermodynamic properties of hydrocarbons. *Proteins* **11,** 281–296 (1991).
41. Esnouf, R. M. An extensively modified version of MolScript that includes greatly enhanced coloring capabilities. *J. Mol. Graph. Model.* **15,** 132–133 (1997).

Supplementary Information accompanies the paper on *Nature*'s website (http://www.nature.com).

Acknowledgements

We thank the staff at the NSLS, Brookhaven National Laboratory, X-25, Cornell High Energy Synchrotron Source, F1 and ALS, Lawrence Berkeley Laboratory, 5.0.2 for synchrotron support; members of the MacKinnon laboratory, P. Model and M. Russel for discussion; C. Miller and D. Gadsby for critical reading of the manuscript; and W. Chin for help in manuscript preparation. This work was supported by grants from the NIH to R.M. and the National Centre for Research Resources, NIH, to B.T.C. R.M. is an investigator in the Howard Hughes Medical Institute.

Competing interests statement

The authors declare that they have no competing financial interests.

Correspondence and requests for materials should be addressed to R.M. (e-mail: mackinn@rockvax.rockefeller.edu). Coordinates have been deposited with the Protein Data Bank under accession code 1LNQ.